

The energy budget and the gravitational wave spectra beyond the bag model

Xiao Wang,^{a,b} Fa Peng Huang,^c Xinmin Zhang^{a,b}

^aTheoretical Physics Division, Institute of High Energy Physics, Chinese Academy of Sciences, 19B Yuquan Road, Shijingshan District, Beijing 100049, China

^bSchool of Physics, University of Chinese Academy of Sciences, Beijing 100049, China

^cDepartment of Physics and McDonnell Center for the Space Sciences, Washington University, St. Louis, MO 63130, USA

E-mail: wangxiao2016@ihep.ac.cn, fapeng.huang@wustl.edu, xmzhang@ihep.ac.cn

Abstract. The energy budget of cosmological first-order phase transition is essential for the production of gravitational wave. Most of previous studies of energy budget are based on the bag model with same sound velocity in the symmetric and broken phase. We study the energy budget and the corresponding gravitational wave spectra beyond the bag model, where the sound speed could be different in the symmetric and broken phase. For a representative effective model, we calculate the sound velocity of different phase, the gravitational wave spectra and signal-to-noise ratio for different combinations of phase transition parameters beyond the bag model. We compare these new results with the ones obtained from the bag model. To give a more precise predictions, the proper sound velocity and phase transition parameters at appropriate temperature are important.

Contents

1	Introduction	1
2	The Equation of State for the hydrodynamics	2
3	Kinetic energy fraction and Efficiency parameter	6
4	The representative effective model	6
5	Gravitational wave signals and signal-to-noise ratio for different sound velocity	10
6	Discussion	12
6.1	The effect of reheating	12
6.2	A fully model-dependent analysis	13
6.3	Multi-step phase transition	15
7	Conclusion	15
A	Fluid profile	17
A.1	Detonation	18
A.2	Deflagration	18
A.3	Hybrid	20
A.3.1	Supersonic deflagration	20
A.3.2	Subsonic detonation	20

1 Introduction

First-order phase transition (FOPT) in the early universe may play important roles in the physical process of baryogenesis, dark matter, primordial magnetic field, primordial black hole, cosmic string, gravitational wave (GW), ect. The generated GW during a strong FOPT through bubble collision, turbulence and sound wave mechanisms could provide new signals to unravel the above problems, and potentially be detected by the future GW experiments, such as LISA [1–4], TianQin [5–7], Taiji [8, 9], Decihertz Interferometer Gravitational wave Observatory (DECIGO) [10, 11], Ultimate-DECIGO(U-DECIGO) [12], and Big Bang Observer (BBO) [13]. Therefore, to clearly understand these fundamental issues in particle physics and cosmology, it is crucial to precisely predict the GW spectra produced by the FOPT process. And the energy budget of cosmological FOPT is essential for precise calculations of GW spectra [14–21]. To obtain the energy budget, it is key to calculate the kinetic energy fraction, which is determined by hydrodynamics of expanding bubble in the plasma, the phase transition strength, the speed of sound in the plasma and the bubble wall velocity. For simplicity, most of previous study use the bag model [14–18, 20], which assumes the symmetric and broken phase share the same constant sound velocity $c_s^2 = 1/3$. However, the phase transition process of a given new physics model could deviate from the bag model, if the some extra particle content obtain field-dependent masses that are comparable with the temperature. And this situation could be general in many extension of the standard model of particle physics.

Therefore, some recent studies consider a situation beyond the bag model [19, 21]. In those works, the symmetric and broken phase can be quantified by a phenomenological equation of state (EOS), and the sound velocity in the two phases could be different.

In this work, we study the different sound velocity model (DSVM) of EOS, which is one simple generalization of the bag model, to explore more reliable energy budget and hydrodynamical processes of this EOS. And the corresponding profiles of the DSVM for different hydrodynamical modes are obtained by solving the fluid equations with different sound velocity in the symmetric and broken phase. Taking the Higgs sextic effective model as an example, we consider the effect of different sound velocities in broken and symmetric phase. Then, based on this effective model we show a concrete calculation of sound velocity, the kinetic energy fraction and other phase transition parameters. With different combination of these phase transition parameters, which are obtained by the bag model of EOS and the DSVM of EOS at different characteristic temperature, we calculate the GW spectra and observe a discrepancy of different parameter combinations. And according to these GW spectra, we also compare signal-to-noise ratio (SNR) of different combinations of phase transition parameters and models of EOS, which are essential for a more reliable prediction.

This paper is organized as the following: In section 2, we discuss the hydrodynamics of the plasma and the corresponding EOS to quantify it. Then, we discuss how to calculate the kinetic energy fraction in section 3. In section 4, we study the Higgs sextic model to do the concrete calculations. And the corresponding GW spectra and signal-to-noise ratio (SNR) of different parameter combinations are investigated in section 5. Discussions and conclusions are given in section 6 and 7. The Appendix gives the fluid profile of three hydrodynamical mode.

2 The Equation of State for the hydrodynamics

To calculate the kinetic energy fraction, we should firstly solve the hydrodynamical equations to get the the fluid profile. We begin our discussion from the energy-momentum tensor of the perfect fluid

$$T^{\mu\nu} = (p + e)u^\mu u^\nu - pg^{\mu\nu} = wu^\mu u^\nu - pg^{\mu\nu} \quad (2.1)$$

where p and e are the pressure and energy density in the local rest frame of the plasma, and $u^\mu = \gamma(1, \mathbf{v})$, with $\gamma = 1/\sqrt{1 - v^2}$, is the four-velocity field. The enthalpy $w = e + p$. These quantities can be obtained from the equilibrium free energy densities in each phase, given by $\mathcal{F}_+(T_+) \equiv \mathcal{F}(\phi_+(T_+), T_+)$ and $\mathcal{F}_-(T_-) \equiv \mathcal{F}(\phi_-(T_-), T_-)$. Thus, the pressure is given by $p = -\mathcal{F}$, the entropy density by $s = dp/dT$, the energy density by $e = Ts - p$, and the enthalpy by $w = e + p = Ts$.

From the energy-momentum conservation $\partial_\mu T^{\mu\nu} = 0$, we can obtain the matching conditions (in the reference frame of the bubble wall) [14–18]

$$w_- v_-^2 \gamma_-^2 + p_- = w_+ v_+^2 \gamma_+^2 + p_+, \quad w_- v_- \gamma_-^2 = w_+ v_+ \gamma_+^2 \quad (2.2)$$

Equivalently, we can obtain the following relations

$$v_+ v_- = \frac{p_+ - p_-}{e_+ - e_-}, \quad \frac{v_+}{v_-} = \frac{e_- + p_+}{e_+ + p_-}. \quad (2.3)$$

Here subscripts + and - indicate the symmetric and broken phase respectively. In literatures, one usually assumes the bag model of EOS to continue the analysis. For the bag model, the

EOS can be written as

$$\begin{aligned} p_+ &= \frac{1}{3}a_+T_+^4 - \epsilon_+, & e_+ &= a_+T_+^4 + \epsilon_+, \\ p_- &= \frac{1}{3}a_-T_-^4 - \epsilon_-, & e_- &= a_-T_-^4 + \epsilon_-. \end{aligned} \quad (2.4)$$

And this introduces the conventional definition of strength parameter [17]

$$\alpha_\theta = \frac{4}{3} \frac{\Delta\epsilon}{w_+}, \quad \epsilon_\pm = \frac{1}{4}(e_\pm - 3p_\pm) \quad (2.5)$$

We use natural units with $c = \hbar = k_B = 1$. In the bag model, the sound velocity of symmetric phase and broken phase are both equals $1/\sqrt{3}$. However, the sound velocity can basically deviate from this value in a realistic FOPT process. In general, the sound velocity should be temperature-dependent.

To more precisely describe the phase transition process, we can assume the sound velocity in both phases is a constant that can deviate $1/\sqrt{3}$. And we can have a relation as $\partial p/\partial e = \text{const}$. Hence the bag model of EOS can be generalized as a DSVM of EOS (which is first studied by ref. [19] with the planer approximation, and also called the ν model [21]). The generalized EOS is

$$\begin{aligned} p_+ &= c_+^2 a_+ T_+^{\nu_+} - \epsilon_+, & e_+ &= a_+ T_+^{\nu_+} + \epsilon_+, \\ p_- &= c_-^2 a_- T_-^{\nu_-} - \epsilon_-, & e_- &= a_- T_-^{\nu_-} + \epsilon_-, \end{aligned} \quad (2.6)$$

where $\nu_\pm = 1 + 1/c_\pm^2$. For $c_\pm^2 = c_\pm^2 = 1/3$, a_- and a_+ are dimensionless and well defined. However, for $c_\pm^2 \neq 1/3$, the coefficient a_\pm is dimensional. Since the bag model of EOS is a special situation of this general model, the temperature-dependent coefficient $a_\pm(T)$ can be defined $a_\pm(T) = a_\pm T^{4-\nu}$, where the dimensionless constant a_\pm is same as the bag model of EOS. Hence when $c_\pm^2 = 1/3$, this model can return to the bag model of EOS. And this model can be rewritten as follow

$$\begin{aligned} p_+ &= c_+^2 a_+ T_+^4 - \epsilon_+, & e_+ &= a_+ T_+^4 + \epsilon_+, \\ p_- &= c_-^2 a_- T_-^4 - \epsilon_-, & e_- &= a_- T_-^4 + \epsilon_-, \end{aligned} \quad (2.7)$$

with $a_\pm = g_\pm \pi^2/30$ (g_\pm is degree of freedom for the symmetric and broken phase) just like the bag model of EOS.

The strength parameter defined in the bag model actually depends on T_+ and T_- . That is $\Delta\epsilon = \epsilon_+(T_+) - \epsilon_-(T_-)$. However, one always use the same temperature (eg. the nucleation temperature) to calculate this quantity. To generalize α_θ without encounter the dependence on the temperature in the broken phase T_- . Ref. [21] expand the thermodynamic quantities around the symmetric phase to derive the corresponding values in the broken phase. And the constant sound velocity give the following relation

$$\frac{v_+}{v_-} = \frac{w_+(v_+v_-/c_-^2 - 1) + \Delta(e - p/c_-^2)}{w_+(v_+v_-/c_-^2 - 1) + v_+v_- \Delta(e - p/c_-^2)} \quad (2.8)$$

Note the Δ represents the differences of various quantities at the same temperature henceforth. Therefore the pseudo-trace definition of the strength parameter is given as [21]

$$\alpha_{\bar{\theta}} = \frac{\Delta\bar{\theta}}{3w_+}, \quad \bar{\theta} = e - p/c_-^2, \quad (2.9)$$

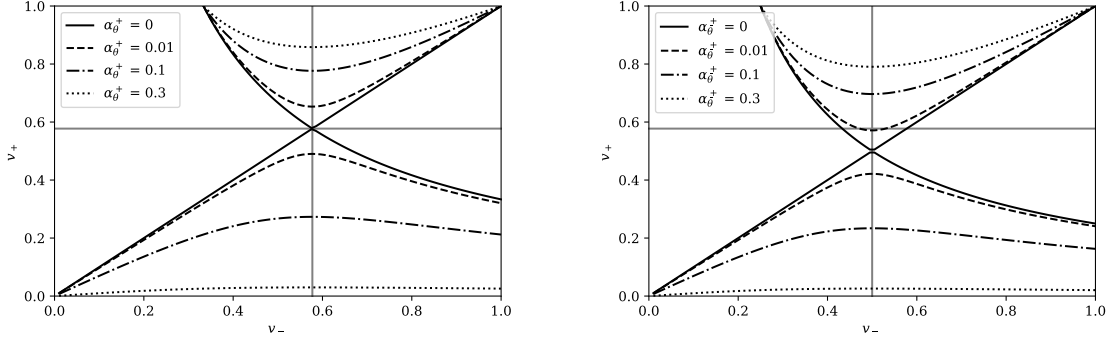


Figure 1. The fluid velocities v_+ and v_- in the reference frame of bubble wall for different definitions and values of phase transition strength parameter. Left panel: the bag model. Right panel: the DSVM with $c_+^2 = 1/3$ and $c_-^2 = 0.25$.

and this can be combined with the matching condition to give

$$v_- = \frac{1}{2v_+(\nu_- - 1)} \left[a \pm \sqrt{c^2 + 4v_+^2(1 - \nu_-)} \right],$$

$$a = 1 - 3\alpha_{\bar{\theta}} + v_+^2(\nu_- + 3\alpha_{\bar{\theta}} - 1), \quad (2.10)$$

and

$$v_+ = \frac{1 - v_-^2(1 - \nu_-) \pm \sqrt{(1 - v_-^2(1 - \nu_-))^2 - 4v_-^2(1 - 3\alpha_{\bar{\theta}})(\nu_- - 1 + 3\alpha_{\bar{\theta}})}}{2v_-(\nu_- - 1 + 3\alpha_{\bar{\theta}})}. \quad (2.11)$$

Hence the \pm signs in eq. (2.11) indicates two branches of solutions. And the two branches of solutions indicate two kinds of hydrodynamical processes may occur during the phase transition process. In the reference frame of the bubble wall, a detonation mode, which is the upper right part of both panel in figure 1, means the incoming flow is faster than the outgoing flow, $v_- < v_+$. And a deflagration mode, which is the bottom left part of both panels in figure 1, indicates the outgoing flow is faster than the ingoing flow, $v_+ < v_-$. Figure 1 shows that v_+ has a minimum at $v_- = c_-$ in the upper right part of both panel, and maximum at $v_- = c_-$ in the bottom left part of both panel. And a mode with $v_- = c_-$ is called Jouguet detonation or deflagration. And the corresponding Jouguet velocity is

$$v_J = \frac{1 \pm \sqrt{3\alpha_{\bar{\theta}}(1 - c_-^2 + 3c_-^2\alpha_{\bar{\theta}})}}{1/c_- + 3c_- \alpha_{\bar{\theta}}} \quad (2.12)$$

where $+$ indicates a Jouguet detonation velocity v_J^{det} , $-$ denotes the Jouguet deflagration velocity v_J^{def} .

A further analysis need deal with the hydrodynamics of the fluid, which is described by the fluid equation. Based on the energy-momentum conservation, we can also derive the fluid equation as [14, 18]

$$\partial_t [(e + pv^2)\gamma^2] + \partial_r [(e + p)\gamma^2 v] = -\frac{j}{r} [(e + p)\gamma^2 v],$$

$$\partial_t [(e+p)\gamma^2 v] + \partial_r [(ev^2+p)\gamma^2] = -\frac{j}{r} [(e+p)\gamma^2] , \quad (2.13)$$

where r denotes the distance from the symmetry plane, axis or point, and t is the duration since nucleation. And $j = 0, 1, 2$ for a planar, cylindrical or spherical bubble configuration, respectively. Since there is no characteristic distance scale in the problem, the solution is similarity solution which depends only on ξ/t . Thus, we can derive

$$\begin{aligned} (\xi - v) \frac{\partial_\xi e}{w} &= j \frac{v}{\xi} + \gamma^2 (1 - v\xi) \partial_\xi v , \\ (1 - v\xi) \frac{\partial_\xi p}{w} &= \gamma^2 (\xi - v) \partial_\xi v . \end{aligned} \quad (2.14)$$

We assume a spherically symmetric configuration in this work,

$$\begin{aligned} (\xi - v) \frac{\partial_\xi e}{w} &= 2 \frac{v}{\xi} + \gamma^2 (1 - v\xi) \partial_\xi v , \\ (1 - v\xi) \frac{\partial_\xi p}{w} &= \gamma^2 (\xi - v) \partial_\xi v . \end{aligned} \quad (2.15)$$

Therefore, the equation that can describe the velocity profile is

$$2 \frac{v}{\xi} = \gamma^2 (1 - v\xi) \left[\frac{\mu^2}{c_s^2} - 1 \right] \partial_\xi v , \quad (2.16)$$

where

$$\mu(\xi, v) = \frac{\xi - v}{1 - \xi v} \quad (2.17)$$

From eq. (2.15) we can also derive the equation for the enthalpy profile,

$$\frac{\partial_\xi w}{w} = \left(1 + \frac{1}{c_s^2} \right) \mu \gamma^2 \partial_\xi v , \quad (2.18)$$

and the equation for temperature profile

$$\frac{\partial_\xi T}{T} = \gamma^2 \mu \partial_\xi v . \quad (2.19)$$

Then we can obtain the enthalpy profile

$$w(\xi) = w_0 \exp \left[\int_{v_0}^{v(\xi)} \left(1 + \frac{1}{c_s^2} \right) \gamma^2 \mu dv \right] , \quad (2.20)$$

and the temperature profile

$$T(\xi) = T_0 \exp \left[\int_{v_0}^{v(\xi)} \gamma^2 \mu dv \right] . \quad (2.21)$$

By solving the above fluid equations and obtain the fluid profiles, we can classify hydrodynamical process of first order phase transition into three stable modes: weak detonation, weak deflagration and hybrid [16–18]. When the bubble wall velocity (v_w) is smaller than the sound speed of the broken phase (c_-), namely $v_w < c_-$, it is called deflagration mode, where the

plasma forms a shock in front of the bubble walls. This mode is favored by the electroweak baryogenesis to guarantee sufficient diffusion time. If the bubble wall velocity is larger than sound velocity of broken phase and smaller than the so-called Jouguet detonation velocity, $c_- < v_w < v_J^{\text{det}}(\alpha_{\bar{\theta}_n})$, it is called the hybrid mode. If the bubble wall velocity is even larger than the Jouguet detonation velocity, it is called the detonation mode, where a rarefaction wave forms behind the bubble walls. Detonation mode usually produces stronger GW signal. The detailed analysis of fluid profile of various hydrodynamical modes are presented in the Appendix. Actually, the GW spectra are proportional to the kinetic energy fraction, which is roughly inversely proportional to the cubic bubble wall velocity. We can see this in the following two sections.

3 Kinetic energy fraction and Efficiency parameter

After solving the hydrodynamical equations and obtain the fluid profile using given EOS, we can further predict the kinetic energy fraction. The kinetic energy fraction K in the fluid can be defined as a fraction of the total energy e [3],

$$K \equiv \frac{\rho_{\text{fl}}}{e_+} = \frac{3}{ev_w^3} \int w(\xi) v^2 \gamma^2 \xi^2 d\xi, \quad \rho_{\text{fl}} = \frac{3}{v_w^3} \int \xi^2 v^2 \gamma^2 w d\xi \quad (3.1)$$

In general, the energy fraction in GWs from sound wave mechanism scales as $h^2 \Omega_{\text{GW}} \propto K^2$ or $h^2 \Omega_{\text{GW}} \propto K^{3/2}$. In most cases, the kinetic energy fraction K for single bubble could be a good approximation of the average for the entire plasma. Since from the detailed discussion in the previous section, the enthalpy profile w and the fluid velocity profile v depend on both the phase transition strength α and the bubble wall velocity v_w , the single bubble kinetic energy fraction also depends on these parameters. According to ref. [21], we choose the pseudo-trace definition of the strength parameter, hence the efficiency parameter can be expressed as

$$\kappa_{\bar{\theta}} = \frac{4\rho_{\text{fl}}}{\Delta\bar{\theta}} \quad (3.2)$$

And the K can be approximated as

$$K \approx \left(\frac{\Delta\bar{\theta}}{4e_+} \kappa_{\bar{\theta}} \right) \quad (3.3)$$

To obtain the energy fraction, we need perform a model dependent calculation of the pre-factor.

4 The representative effective model

In this section, we take an representative effective model, the Higgs sextic model [23–27] with the tree-level potential $V(\phi) = \frac{\mu^2}{2}\phi^2 + \frac{\lambda}{4}\phi^4 + \frac{\kappa}{8\Lambda^2}\phi^6$, to make precise predictions on the sound speed, the phase transition dynamics and parameters. This effective model is a generic prediction for many new physics models motivated by dark matter, baryogenesis and so on. From the perspective of standard model effective field theory, this Higgs sextic operator could naturally appear after the heavy degrees of freedom are integrated out in the new physics model, such as scalar extended Higgs model or composite Higgs model [27]. Meanwhile, other dimension-six operators could also appear simultaneously and contribute to the oblique

observables. They can suffer from the condition of strong FOPT and the electroweak precise measurements. Since we focus on the investigation of the fluid profile and phase transition dynamics, we can only study the Higgs sextic term with the leading-order thermal corrections.

$$V_{\text{eff}}(\phi, T) \approx \frac{\mu^2 + cT^2}{2}\phi^2 + \frac{\lambda}{4}\phi^4 + \frac{\kappa}{8\Lambda^2}\phi^6, \quad (4.1)$$

where $\Lambda/\sqrt{\kappa}$ is the effective cutoff scale and c is the thermal correction

$$c = \frac{1}{16}(g'^2 + 3g^2 + 4y_t^2 + 4\frac{m_h^2}{v^2} - 12\frac{\kappa v^2}{\Lambda^2}). \quad (4.2)$$

g' , g , y_t , v is the $U(1)$ gauge coupling, $SU(2)$ gauge coupling, top quark Yukawa coupling, and electroweak vacuum expectation value (VEV), respectively. In this model, the free energy can be expressed as

$$\mathcal{F}(\phi, T) = V_{\text{eff}}(\phi, T) \approx -\frac{a_+}{3}T^4 + \frac{\mu^2 + cT^2}{2}\phi^2 + \frac{\lambda}{4}\phi^4 + \frac{\kappa}{8\Lambda^2}\phi^6. \quad (4.3)$$

Here, we include the field-independent term $-\frac{a_+}{3}T^4$, which is omitted in the discussions of the phase transition dynamics and parameters. This term is needed to calculate the sound speed. We can obtain the sound velocity of broken and symmetric phase, then match this to the DSVM. In general, the sound velocity is given as

$$c_s^2 = \left. \frac{\partial p / \partial T}{\partial e / \partial T} \right|_{T=T_*} \quad (4.4)$$

where $p = -V_{\text{eff}}$ and $e = T\frac{\partial p}{\partial T} - p$. For this model, we can derive the sound velocity

$$c_s^2 = \left. \frac{4a_+T^3 - 3cT\phi^2}{12a_+T^3 - 3cT\phi^2} \right|_{T=T_*}. \quad (4.5)$$

where the value of ϕ is zero in symmetric phase. However, the value for broken phase is

$$\phi_{\text{true}} = \sqrt{\frac{-2\lambda\Lambda^2 + 2\Lambda\sqrt{\lambda^2\Lambda^2 - 3\kappa(\mu^2 + cT^2)}}{3\kappa}}. \quad (4.6)$$

and the phase transition strength parameter can be obtained as

$$\alpha_{\bar{\theta}_n} = \frac{(1 + 1/c_-^2)\Delta V_{\text{eff}} - T\frac{\partial\Delta V_{\text{eff}}}{\partial T}}{3(1 + c_+^2)\rho_{\text{R}}}, \quad \rho_{\text{R}} = a_+T_+^4 \quad (4.7)$$

From above equations, we find the sound velocity is actually temperature-dependent. Hence choosing different temperature can give a different efficiency parameter.

The conventional definition of the phase transition strength parameter based on the bag model of EOS can be written as

$$\alpha_{\theta} = \frac{\Delta V_{\text{eff}} - \frac{T}{4}\frac{\partial\Delta V_{\text{eff}}}{\partial T}}{\rho_{\text{R}}}. \quad (4.8)$$

This definition is based on the same sound speed (ie. $c_{\pm} = 1/\sqrt{3}$) approximation in the broken and symmetric phase. And for this bag model and definition of phase transition strength parameter, we can derive the kinetic energy fraction as

$$K_{\theta} = \frac{\alpha_{\theta}\kappa_{\theta}}{1 + \alpha_{\theta}}. \quad (4.9)$$

Considering different sound velocities in both phase, the more realistic kinetic energy fraction should be modified as

$$K_{\bar{\theta}} = \frac{\Delta\bar{\theta}}{4e_{+}}\kappa_{\bar{\theta}}. \quad (4.10)$$

For the Higgs sextic model, $e_{+} = a_{+}T^4/3$ in symmetric phase, we can obtain

$$K_{\bar{\theta}} = \frac{9}{16}(1 + c_{+}^2)\alpha_{\bar{\theta}}\kappa_{\bar{\theta}} \quad (4.11)$$

where $c_{+}^2 = 1/3$. Hereafter, we use θ to represent the parameters calculated using the bag model with $c_{\pm}^2 = 1/3$. And we use $\bar{\theta}$ to represent the quantities derived from the DSVM of EOS with different sound velocity in the symmetric and broken phase.

In table 1, we list the important phase transition parameters of different benchmark points. We only consider the detonation case for simplicity with the bubble wall velocity $v_w = 0.95$. From this table, we can observe that for the DSVM, the sound velocity in the broken phase is different for different cut-off scale. Basically, lower cut-off gives smaller sound velocity, and the deviation from the bag model is more obvious. And the precise definition of these phase transition parameters can be find in our previous study [22], we give a brief explanation of these parameters in the following.

T_n is the nucleation temperature at which one bubble is nucleated in one Hubble radius. 34% of false vacuum has been converted to true vacuum at the percolation temperature T_p , at which a large fraction of bubbles collide and percolate. $\alpha_{\bar{\theta}_n}$ is the phase transition strength given by the DSVM of EOS at the nucleation temperature. α_{θ_n} is the phase transition strength given by the bag model at the nucleation temperature. At the percolation temperature, $\alpha_{\bar{\theta}_p}$ and α_{θ_p} are the phase transition strength derived by the DSVM of EOS and the bag model respectively. $\tilde{\beta}_n$ and $\tilde{\beta}_p$ represent the value of phase transition duration obtained at the nucleation and percolation temperature respectively. HR_p quantifies the mean bubble separation at the percolation temperature. We can basically use the time duration parameter $\tilde{\beta}$ to approximate it [22]. In the broken phase, the values of sound velocity for nucleation and percolation temperature are denoted by c_{-n}^2 and c_{-p}^2 . According to the DSVM, we can derive the efficiency parameter at nucleation and percolation temperature as $\kappa_{\bar{\theta}_n}$ and $\kappa_{\bar{\theta}_p}$. Then we can subsequently obtain the corresponding kinetic energy fraction, $K_{\bar{\theta}_n}$ and $K_{\bar{\theta}_p}$. For the bag model, we can also derive the efficiency parameter, κ_{θ_n} and κ_{θ_p} , and the kinetic fraction, K_{θ_n} and K_{θ_p} , at the nucleation and percolation temperature.

For this Higgs sextic effective model, we show the evolution of the sound speed with the temperature in the broken phase for different cut-off scales in figure 2. With the decreasing of the temperature, the sound velocity also decreases, and is smaller than the sound velocity in pure radiation phase $c_s = 1/\sqrt{3}$. Since the kinetic energy fraction or EOS depends on the sound speed in two phases, any deviation from c_s might have some effects on the kinetic energy fraction. In our previous study [22], we classify the FOPT into four classes, slight supercooling for $\alpha < 0.1$, mild supercooling for $0.1 < \alpha < 0.5$, strong supercooling for $0.5 < \alpha < 1$ and ultra supercooling for $\alpha > 1$. For strong supercooling and ultra supercooling,

	BP_1	BP_2	BP_3	BP_4	BP_5	BP_6
$\Lambda/\sqrt{\kappa}$ [GeV]	620	610	600	590	587	586
T_n [GeV]	65.286	60.153	53.581	43.454	38.118	35.399
T_p [GeV]	64.032	58.751	51.738	40.538	34.364	30.795
$\alpha_{\bar{\theta}_n}$	0.0436	0.0621	0.102	0.252	0.444	0.612
α_{θ_n}	0.0435	0.0617	0.101	0.247	0.430	0.588
$\alpha_{\bar{\theta}_p}$	0.0484	0.0701	0.121	0.346	0.704	1.129
α_{θ_p}	0.0481	0.0695	0.120	0.336	0.674	1.066
$\tilde{\beta}_n$	1023.948	722.848	438.429	177.375	97.708	62.392
$\tilde{\beta}_p$	799.409	652.238	326.527	129.352	50.517	11.879
HR_p	0.00490	0.00884	0.0117	0.0276	0.0628	0.114
c_{-n}^2	0.3174	0.3140	0.3080	0.2927	0.2788	0.2688
c_{-p}^2	0.3166	0.3128	0.3058	0.2857	0.2641	0.2442
$\kappa_{\bar{\theta}_n}$	0.0578	0.0783	0.117	0.220	0.300	0.345
$\kappa_{\bar{\theta}_p}$	0.0634	0.0866	0.133	0.265	0.364	0.415
$K_{\bar{\theta}_n}$	0.00189	0.00364	0.00895	0.0416	0.0999	0.158
$K_{\bar{\theta}_p}$	0.00230	0.00455	0.0121	0.0688	0.192	0.351
κ_{θ_n}	0.0626	0.0865	0.134	0.276	0.403	0.485
κ_{θ_p}	0.0688	0.0964	0.156	0.344	0.521	0.641
K_{θ_n}	0.00261	0.00503	0.0123	0.0548	0.121	0.179
K_{θ_p}	0.00316	0.00626	0.0167	0.0864	0.210	0.330

Table 1. Phase transition parameters of different benchmark points for different definitions and different models of EOS. We only consider the detonation case with the bubble wall velocity $v_w = 0.95$ for simplicity.

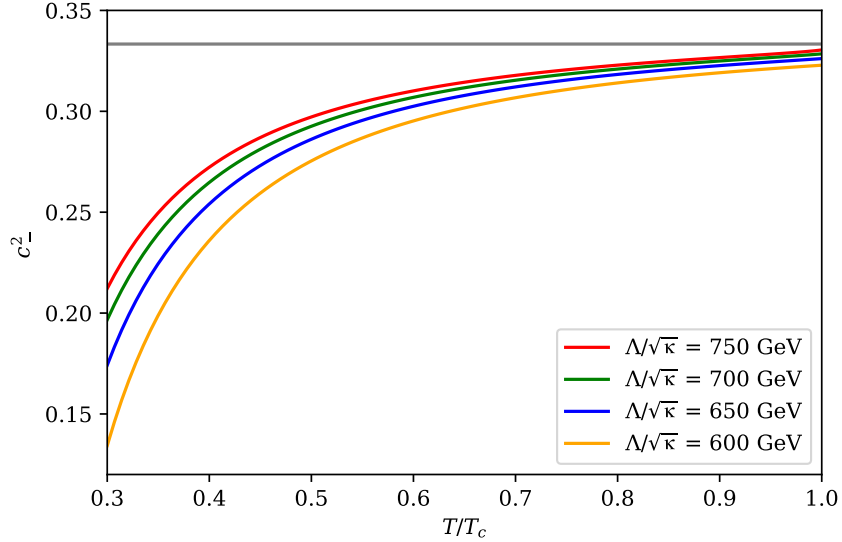


Figure 2. The evolution of the sound speed with the temperature in the broken phase for different cut-off scales.

the nucleation temperature is obviously smaller than the critical temperature. Therefore, the velocity deviation, which can be observed in table 1, becomes more obvious for strong supercooling and ultra supercooling.

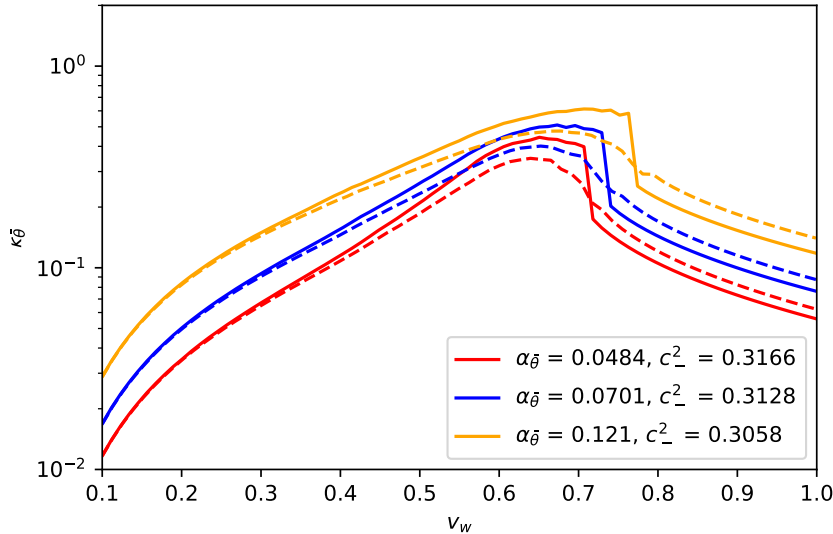


Figure 3. Illustration of the efficiency parameter for the bag model and the DSVM. The dashed line and the solid line show the efficiency parameter of the bag model and the DSVM with the same phase transition strength respectively.

For different cut-off, we can derive the nucleation temperature and the sound velocity. In figure 3, we show the efficiency parameter for the bag model and the DSVM. The dashed line and the solid line show the efficiency of the bag model and the DSVM respectively with the same phase transition strength. We can see that even for small deviation of the sound velocity, there exist differences of the efficiency factor between bag model and the DSVM. For smaller cutoff, the deviation will be more obvious. Besides the bubble wall velocity, the efficiency factor also depends on the phase transition strength parameter and the sound velocity in each phase for DSVM. Basically, we can also find the efficiency parameter of the DSVM is slightly larger than the bag model for the deflagration and hybrid mode. While it is smaller than the bag model for the detonation mode.

5 Gravitational wave signals and signal-to-noise ratio for different sound velocity

In this section, we precisely calculate the GW spectra for the Higgs sextic effective scenario by precise calculation of the kinetic energy fraction and energy budget in the case of different sound velocity. There are three mechanisms to produce GWs during a FOPT, the bubble collision, turbulence and sound wave. In most realistic models, sound wave mechanism produces stronger signals than bubble collision and turbulence. For sound wave, the energy fraction in GWs scales as $\Omega_{\text{GW}} \propto K^2$ or $\Omega_{\text{GW}} \propto K^{3/2}$ for $H_*\tau_{sh} < 1$, where τ_{sh} is the shock formation time.

More precisely, for bubble wall velocity away from the Jouguet detonation speed, we have [3].

$$\frac{d\Omega_{\text{GW}}}{d\ln f} = 0.687 F_{\text{GW}} K^2 (H_* R_*/c_s) C \left(\frac{f}{f_p} \right) \eta, \quad (5.1)$$

where the coefficient $\eta \sim 10^{-2}$, and

$$F_{\text{GW}} = (3.57 \pm 0.05) \times 10^{-5} \left(\frac{100}{g_*} \right)^{\frac{1}{3}}. \quad (5.2)$$

The spectral shape function is

$$C(s) = s^3 \left(\frac{7}{4 + 3s^2} \right)^{\frac{7}{2}}, \quad (5.3)$$

with the peak frequency

$$f_p \simeq 26 \left(\frac{1}{H_* R_*} \right) \left(\frac{z_p}{10} \right) \left(\frac{T_*}{100 \text{ GeV}} \right) \left(\frac{g_*}{100} \right)^{\frac{1}{6}} \mu\text{Hz}. \quad (5.4)$$

T_* can be the nucleation temperature T_n or the percolation temperature T_p . H_* and R_* is the Hubble parameter and the mean bubble separation calculated at the nucleation temperature T_n or the percolation temperature T_p . The quantity $z_p \approx 10$ is determined from simulations [3]. g_* is the effective degree of freedom at T_* . When we consider the sound wave, the contributions from bubble collision and turbulence are much smaller, and can be neglected.

If $\tau_{sh} H_* < 1$, the GW spectra is suppressed and can be written as [3].

$$\frac{d\Omega_{\text{GW}}}{d \ln f} = 0.687 F_{\text{GW}} K^{3/2} (H_* R_* / \sqrt{c_s})^2 C \left(\frac{f}{f_p} \right) \eta. \quad (5.5)$$

For the suppressed sound wave spectra, the contributions from turbulence and bubble collision may not be negligible. Then we might include the GW spectra for turbulence and bubble collisions.

According to the numerical calculations, we find $\tau_{sh} H_* < 1$ for all benchmark points of the Higgs sextic model. Thus, we should use the suppressed GW spectra in eq. (5.5). And we find the turbulence can have non-negligible contribution. The GW spectrum from bubble collision is too small and can be neglected in our numerical results. Based on the kinetic energy fraction and other phase transition parameters derived from the bag model and the DSVM respectively, we show the GW spectra for the six different benchmark points with different combinations of the phase transition parameters and models of EOS in figure 4. The colored regions represent the expected sensitivity for the future GW experiments, LISA [1–4], TianQin [5–7], Taiji [8, 9], DECIGO [10, 11], U-DECIGO [12], BBO [13]. The signals for most of the benchmark are within the sensitivities of LISA, Taiji, DECIGO, U-DECIGO, and BBO. The GW spectra, derived with different combination of phase transition parameter for different characteristic temperature, could have a hierarchy that can reach at most two orders of magnitude. However the spectra show that there are slightly differences between the combinations that are derived by different EOS for the same temperature.

To clearly quantify whether the signal is detectable by a given GW experiment, we should also estimate the SNR for each case using the following formula,

$$\text{SNR} = \sqrt{\mathcal{T} \int_{f_{\min}}^{f_{\max}} df \left[\frac{h^2 \Omega_{\text{GW}}(f)}{h^2 \Omega_{\text{det}}(f)} \right]^2}, \quad (5.6)$$

where \mathcal{T} is the total observation time and $h^2 \Omega_{\text{det}}(f)$ is the nominal sensitivity of a given GW experiment configuration to cosmological sources. For simplicity, we assume 4 years mission

	$\alpha_{\theta n} \tilde{\beta}_n$	$\alpha_{\theta p} \tilde{\beta}_p$	$\alpha_{\bar{\theta} n} \tilde{\beta}_n$	$\alpha_{\bar{\theta} p} \tilde{\beta}_p$	$\alpha_{\theta p} HR_p$	$\alpha_{\bar{\theta} p} HR_p$
SNR _(LISA)	7.949	16.930	5.979	14.969	16.009	14.043
SNR _(Taiji)	14.759	58.607	11.071	51.524	66.216	58.086
SNR _(TianQin)	0.451	1.506	0.339	1.325	1.629	1.429

Table 2. The SNR of BP_5 for different experiment configuration with different combinations of phase transition parameters and models of EOS

	$\alpha_{\theta n} \tilde{\beta}_n$	$\alpha_{\theta p} \tilde{\beta}_p$	$\alpha_{\bar{\theta} n} \tilde{\beta}_n$	$\alpha_{\bar{\theta} p} \tilde{\beta}_p$	$\alpha_{\theta p} HR_p$	$\alpha_{\bar{\theta} p} HR_p$
SNR _(LISA)	14.229	15.367	11.887	16.639	17.367	19.029
SNR _(Taiji)	38.665	427.813	32.152	468.653	213.123	233.514
SNR _(TianQin)	1.060	5.569	0.882	6.098	3.972	4.352

Table 3. The SNR of BP_6 for different experiment configuration with different combinations of phase transition parameters and models of EOS.

duration time with a duty cycle of $75\%T$, and take $T \simeq 9.46 \times 10^7$ s. In tables 2 and 3, we list the SNR of BP_5 and BP_6 for different experiment configuration with different combinations of phase transition parameters, respectively. We can see that LISA, TianQin, Taiji are capable to detect the signals for enough observation time. The SNR of BP_6 is larger than the SNR in BP_5 . For each benchmark point, there exists obvious modification to the SNR for different parameter combination. Therefore, to obtain more precise predictions on the SNR of the GW signal, it is important to choose a proper phenomenological EOS for the plasma, which can approximately describe the phase transition process, and the parameter combinations at appropriate temperature.

6 Discussion

6.1 The effect of reheating

During a FOPT process, the liberated energy is not fully converted into the kinetic energy of the surrounding fluid. Hence the kinetic energy fraction is smaller than $\mathcal{O}(1)$. In fact the rest of the liberated energy reheats the fluid that surrounding the expanding bubble wall. Based on the DSVM, we can derive the temperature profile with eq. (2.21). Figure 5 depicts the temperature profile of three hydrodynamical modes which are weak deflagration, hybrid, and weak detonation respectively, and show reheating phenomenon of the expanding bubble wall. The two plots in the top of figure 5 represent the temperature profiles of deflagration and hybrid with different sound velocity of the symmetric and broken phase. And these plots show the lower sound velocity of both phase can enhance the reheating effect in front of the bubble wall. The bottom panel of figure 5 shows the temperature profile of detonation mode. And we find the reheating effect can only be altered by changing the sound speed of the broken phase. Decreasing the sound speed of the broken phase weakens the reheating effect of detonation mode. In section 4, we calculate the sound speed of the broken phase with nucleation and percolation temperature for simplicity. A more precise approach to compute the sound velocity is using the temperature far behind the wall, which can be derived by solving the temperature profile. However, figure 5 shows that the temperature far behind the wall is not significantly different from the nucleation temperature for detonation mode. Therefore, we can use nucleation temperature or the percolation temperature as a proper approximation

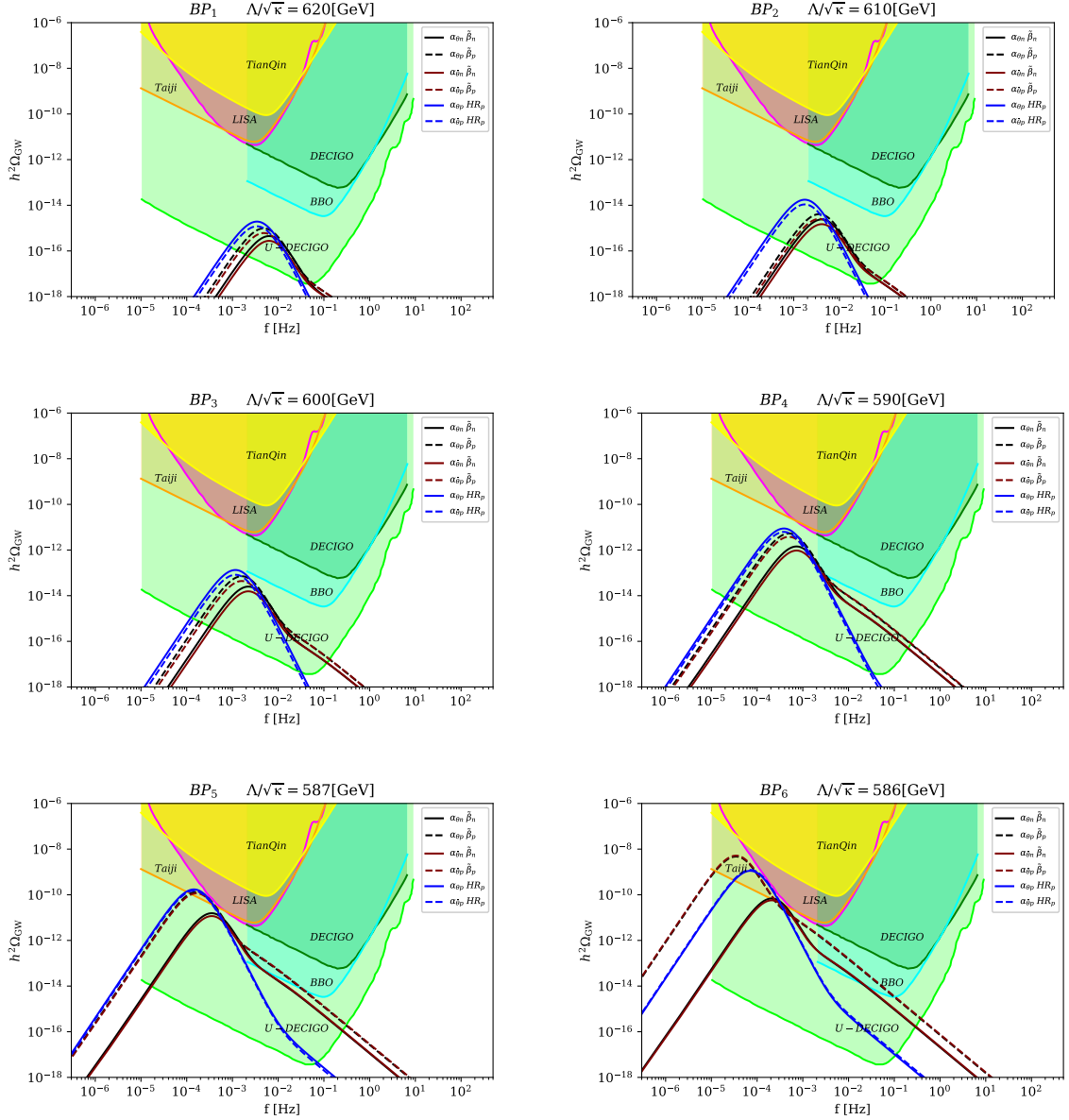


Figure 4. Gravitational wave spectra for the six benchmark points with different definitions of phase transition parameters and different models of EOS. The colored regions represent the expected sensitivity for the future GW experiments, LISA, TianQin, Taiji, DECIGO, U-DECIGO, and BBO.

of the temperature of the broken phase. For the deflagration mode, the reheating effect just in front of the wall may give some influences to the baryogenesis, which is studied in ref. [28].

6.2 A fully model-dependent analysis

The key point of the analysis shown in section 4 is to match a realistic model on a benchmark EOS (the DSVM of EOS is applied in this work), this can give a model-independent approach that simplify the study of phase transition. However, the accuracy of this method depend on whether the benchmark EOS can describe the phase transition process appropriately. In a

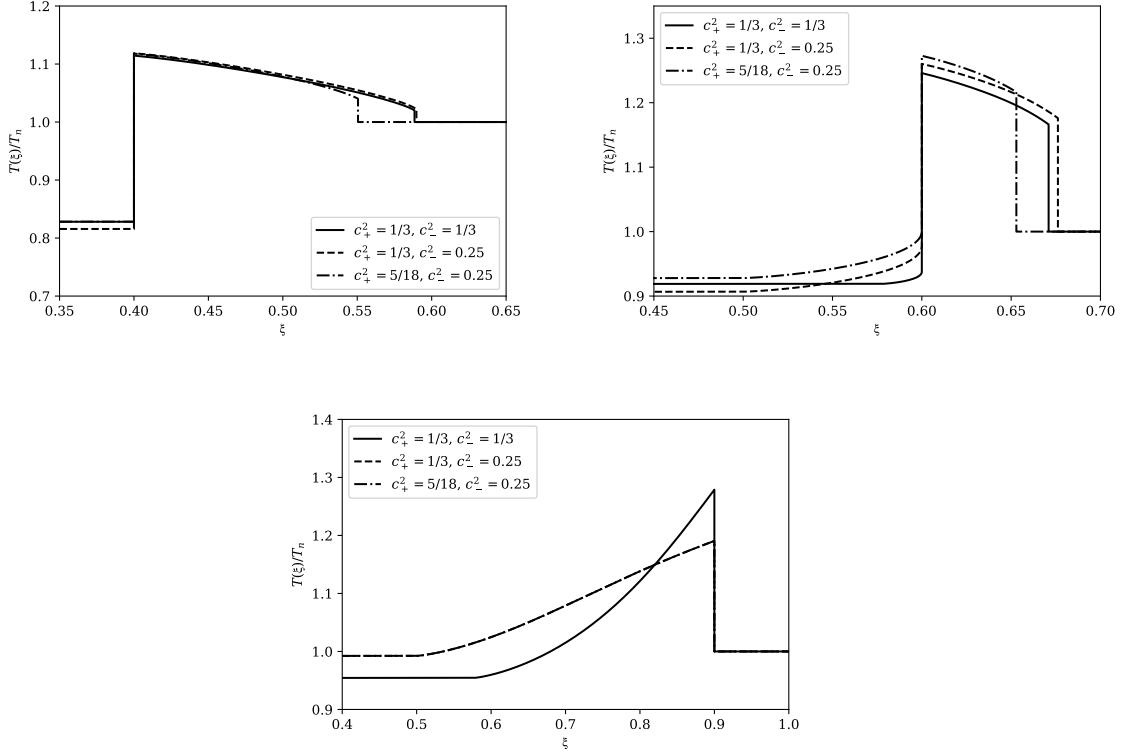


Figure 5. The temperature profile of the three hydrodynamical modes: weak deflagration, hybrid and weak detonation

realistic phase transition process, the sound velocity should be temperature dependent. Due to the reheating effect, the temperature is position dependent, hence the sound velocity is eventually position dependent. And this should make the fluid equation more complicated, but we can use a fully numerical calculation to derive corresponding quantities. Here we exemplify this model-dependent analysis, and leave a further study to a future work. For a given model, we can derive its free energy as

$$\mathcal{F}(\phi, T) = V_{\text{eff}}(\phi, T) = V_T(\phi, T) + V_0(\phi, T) , \quad (6.1)$$

and according to the free energy we can obtain the EOS

$$p = -V_T - V_0, \quad e = -T \frac{\partial V_T}{\partial T} + V_T + V_0 . \quad (6.2)$$

Based on this EOS we can perform the same analysis in this work, and give the corresponding prediction of GW signals and SNR.

For the precise calculations of the GW spectra, there is another important parameter, the bubble wall velocity, which affects the results significantly. Since in most studies, the bubble wall velocity is taken as an input parameter. And the GW spectra strongly depend on the bubble wall velocity, namely, the kinetic energy fraction inversely proportional to cubic wall velocity. In principle, this bubble wall velocity can be calculated by solving the EOM for the phase transition order-parameter fields and the collision terms for a given new physics model. It is also model dependent. Work on more precise kinetic energy fraction and GW spectra with more realistic calculation of the bubble wall velocity [29] is in progress.

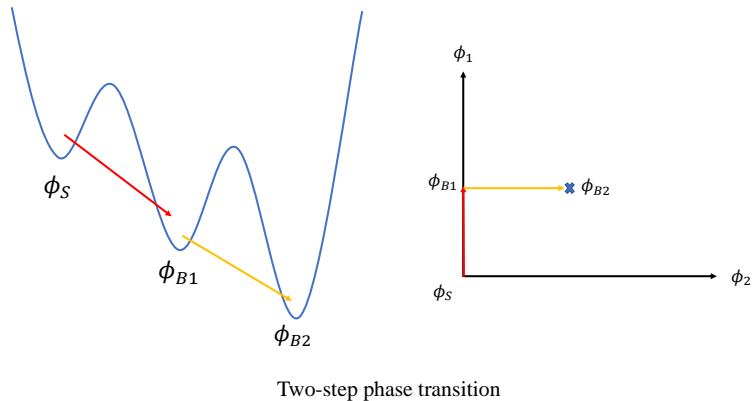


Figure 6. Illustration of the two-step phase transition process.

6.3 Multi-step phase transition

For a given new physics model with N scalar fields ($N > 1$), each scalar field can obtain a VEV and there could occur multi-step FOPTs in the N scalar space. Here we take a two-step phase transition as an example, the first step phase transition is the same as the one-step phase transition. Illustration of the two-step phase transition process is shown in figure 6. However, the second phase transition shows some differences. For example, the sound velocity in ϕ_{B1} phase deviates from $1/\sqrt{3}$. Especially for the phase transitions with bubbles nucleated inside the bubbles [30, 31], the effects of different sound speed may be even more important. In this case, the EOS and sound speed in each phase may have significant differences.

7 Conclusion

Taking the Higgs sextic effective model as a representative model for a generic new physics models, we have calculated the kinetic energy fraction by solving the hydrodynamics equations and the fluid profile beyond the bag model approximation for the two phase of the plasma. Based on the different sound velocity model, which is a simple generalization of the bag model, different sound velocities can be presented in symmetric and broken phase. Choosing proper phase transition parameters, characteristic temperature and more realistic model of EOS, we can give more precise and reliable predictions of the GW signal. The different sound velocity of broken phase can significantly affect the detectability of the GW signal. The approach shown in this work could help the future GW experiments to unravel the underlying physics by matching the precise spectra prediction to the data, and could be directly used in other new physics models with strong FOPT.

Acknowledgments

FPH thanks Yi-Ming Hu and Zheng-Cheng Liang's helpful discussions and providing the updated sensitivity of TianQin project. FPH is supported in part by the McDonnell Center for the Space Sciences. XW and XMZ are supported in part by the Ministry of Science and

Technology of China (2016YFE0104700), the National Natural Science Foundation of China (Grant NO. 11653001), the CAS pilot B project (XDB23020000).

Note added. While this paper was under completion, we notice ref. [35] appeared on arXiv, partially overlapping with this work.

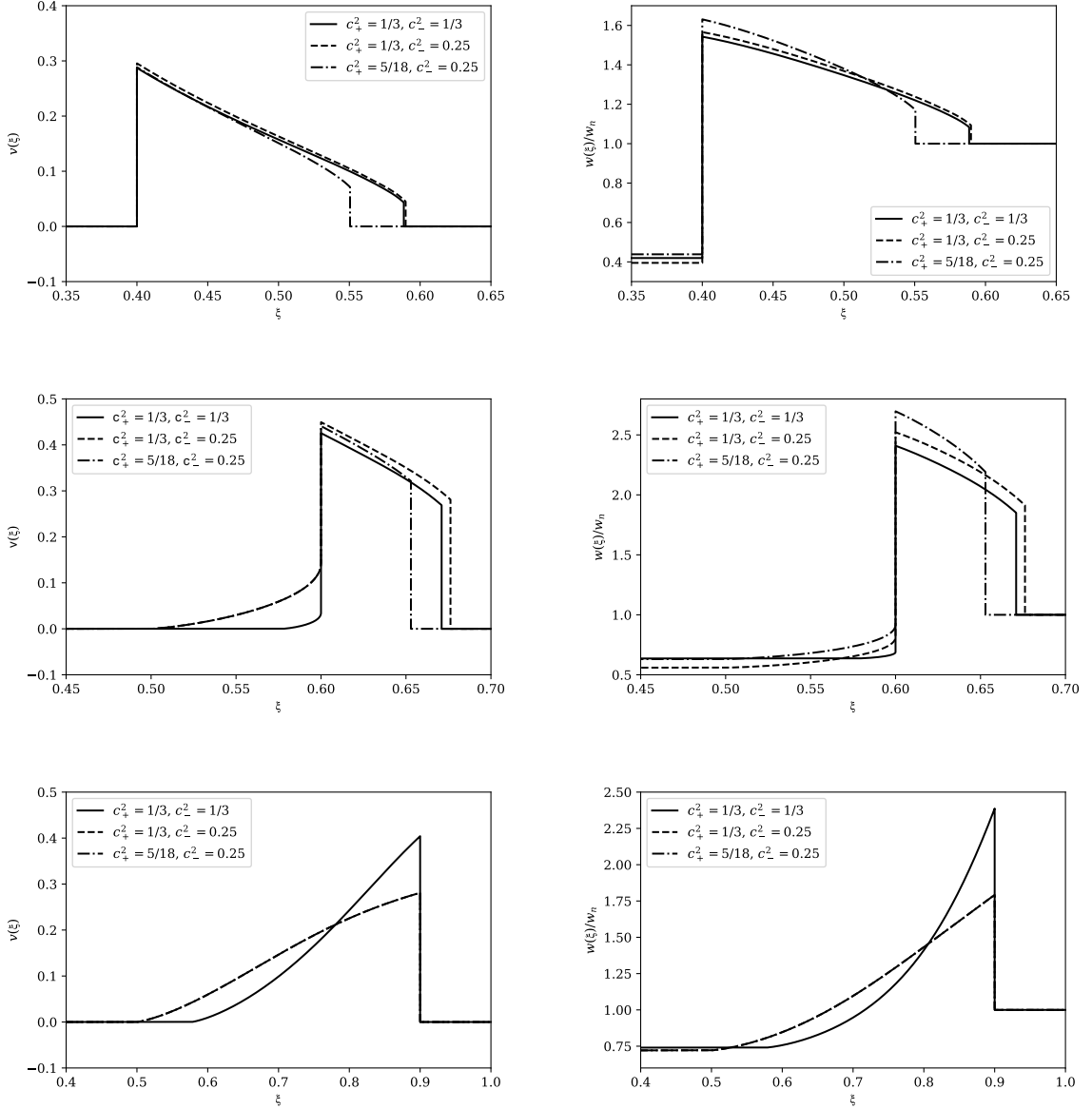


Figure 7. Velocity and enthalpy profile for the weak deflagration ($v_w = 0.4$), hybrid ($v_w = 0.6$) and weak detonation ($v_w = 0.9$) with $\alpha_{\bar{\theta}n} = 0.3$.

A Fluid profile

As shown in figure 1, the hydrodynamical processes can be roughly divided into two kinds, which are detonation ($v_- < v_+$) and deflagration ($v_+ > v_-$). And we can further divided this two kinds into six modes, which are weak detonation, strong detonation, Jouguet detonation, weak deflagration, strong deflagration, and hybrid. However, the stability analysis [32–34] shows only three kinds of modes can be realized in a FOPT process, namely, weak detonation, weak deflagration, and hybrid. In the following, we describe these modes and show the velocity and enthalpy profile with $\alpha_{\bar{\theta}n} = 0.3$ in figure 7.

A.1 Detonation

For the bubble wall moves with $v_w > v_J^{\text{det}}(\alpha_{\bar{\theta}_n})$, we have a weak detonation mode. In this the case, the fluid is unperturbed in front of the bubble wall in the reference frame of the plasma, we have $\tilde{v}_+ = 0$ (v and \tilde{v} represent the fluid velocity in the wall frame and the plasma frame respectively). Hence we have $v_w = v_+$, and the fluid velocity behind the wall must have a velocity $\tilde{v}_- > 0$. Therefore, the boundary conditions to solve the profile of detonation mode can be obtained as

$$\tilde{v}_+ = 0, \quad v_+ = \xi_w, \quad v_- = v_-(\alpha_{\bar{\theta}_+}, v_+), \quad v(\xi_w) = \tilde{v}_- = \mu(\xi_w, v_-) \quad (\text{A.1})$$

And here we have $\alpha_{\bar{\theta}_n} = \alpha_{\bar{\theta}_+}$. Using the boundary conditions for the enthalpy profile $w_+ = w_n$ and the velocity v_-, v_+ derived above, based on the second equations of the matching condition, we can obtain the enthalpy just behind the bubble wall as

$$w_- = w_+ \left(\frac{\xi_w}{1 - \xi_w^2} \right) \left(\frac{1 - v_-^2}{v_-} \right) \quad (\text{A.2})$$

And from eqs. (2.7), we can derive

$$w_+ = (1 + c_+^2) a_+ T_+^4. \quad (\text{A.3})$$

Since $T_+ = T_n$ for the detonation mode, we need use the following relations to obtain T_- .

$$\frac{w_n}{w_-} = \frac{a_+ T_+^4}{a_- T_-^4} \quad (\text{A.4})$$

To determine T_- , a_+ and a_- should be fixed. Based on the Higgs sextic effective model we assume the particle content in the symmetric phase is the standard model particles and the top quark and Higgs boson decouple from the plasma in the broken phase. Hence we have $a_+ = 106.75\pi^2/30$ and $a_- = 95.25\pi^2/30$. The velocity and enthalpy profile of detonation mode with different sound velocities are shown in bottom panel of figure 7.

A.2 Deflagration

If the bubble wall is subsonic with respect to the reference frame of plasma, $v_w < c_-$, we have a deflagration mode. As shown in figure 8, the deflagration mode should form a shock front which is in front of the bubble wall. Here v_1 and v_2 is the fluid velocity behind and in front of the shock front with respect to the shock front frame. The index 1 is for quantities behind the shock and the index 2 is for quantities in front of the shock. From eqs. (2.7), we have the following relations

$$v_1 v_2 = \frac{p_2 - p_1}{e_2 - e_1}, \quad \frac{v_1}{v_2} = \frac{e_2 + p_1}{e_1 + p_2}. \quad (\text{A.5})$$

Since the shock wave is in the symmetric phase, the EOS is the same on the both side of shock front, we have

$$v_1 v_2 = c_+^2, \quad \frac{v_1}{v_2} = \frac{T_2^4 + c_+^2 T_1^4}{T_1^4 + c_+^2 T_2^4}. \quad (\text{A.6})$$

And for the shock front it has been proven that $v_1 < c_+ < v_2$ [17–19]. Hence in the plasma frame, we have $\tilde{v}_1 = \mu(v_{sh}, v_1) > \tilde{v}_2 = \mu(v_{sh}, v_2)$. Since in the plasma frame the fluid velocity

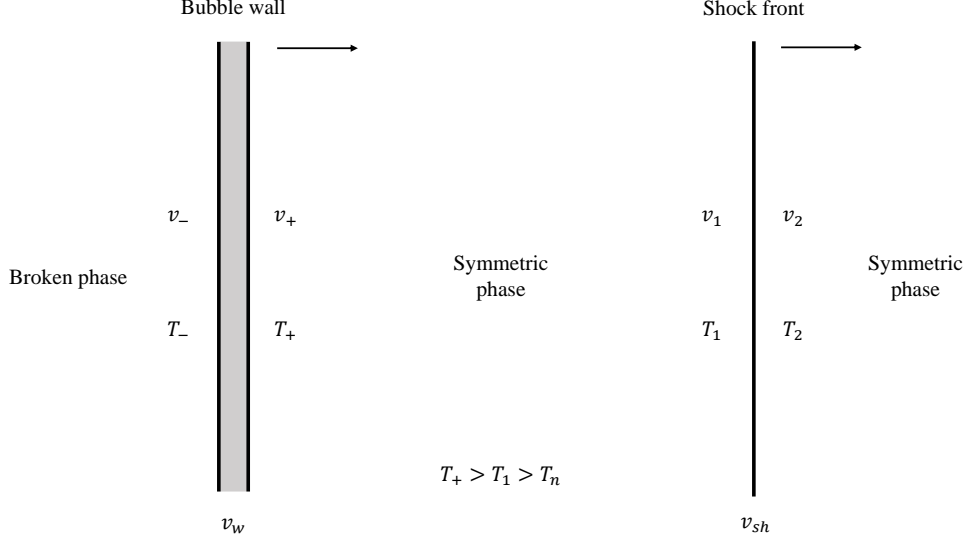


Figure 8. An illustration of the deflagration mode. For the detonation mode, the shock front should disappear.

should vanish in front of the shock, we have $v_2 = v_{sh}$. Hence, the following relation can be derived from eqs. A.6,

$$v_{sh} = \frac{1 - c_+^2}{2} \tilde{v}_1 + \sqrt{\left(\frac{1 - c_+^2}{2} \tilde{v}_1\right)^2 + c_+^2}. \quad (\text{A.7})$$

This condition determines the position of the shock front, which occurs before the singular point $\mu(\xi, v) = c_+$ is reached, and show that $v_{sh} > c_+$. From the second equation of eqs. A.6, we can derive

$$\left(\frac{T_2}{T_1}\right)^4 = \frac{w_2}{w_1} = \frac{c_+^2(1 - v_{sh}^2)}{v_{sh}^2 - c_+^4}, \quad (\text{A.8})$$

where $T_2 = T_n$, $w_n = w_2$.

As shown in the above, the bubble wall of the deflagration mode is preceded by a shock front, hence behind the wall the fluid velocity should also vanish with respect to the plasma frame. Therefore, we have $\tilde{v}_- = 0$ and $v_+ < v_- = v_w < c_-$. We can choose the fluid velocity \tilde{v}_+ (just in front of the bubble wall) and \tilde{v}_1 (behind the shock front) as the initial condition for the fluid equation. Here we choose \tilde{v}_+ as the initial condition, and it can be derived from the following relations,

$$\tilde{v}_- = 0, \quad v_- = v_w, \quad v_+ = v_+(\alpha_{\bar{\theta}_+}, v_-), \quad \tilde{v}_+ = \mu(v_w, v_+) \quad (\text{A.9})$$

Note that $\alpha_{\bar{\theta}_+} \neq \alpha_{\bar{\theta}_n}$ for deflagration mode, since the shock wave reheats the plasma in front of the bubble wall. Hence we should firstly find v_{sh} and $\alpha_{\bar{\theta}_+}$ with

$$\frac{\alpha_{\bar{\theta}_+}}{\alpha_{\bar{\theta}_n}} = \frac{w_n}{w_+}, \quad (\text{A.10})$$

and w_+ can be given by eq. (2.21),

$$\frac{w_1}{w_+} = \exp \left[\int_{\tilde{v}_+}^{\tilde{v}_1} \left(1 + \frac{1}{c_+^2} \right) \gamma^2 \mu dv \right], \quad (\text{A.11})$$

where w_1 can be obtain by eq. (A.8). The velocity and enthalpy profile of deflagration mode is shown in top panel of figure 7.

A.3 Hybrid

For the different sound velocity model, the hybrid can be further divided into two modes, which are supersonic deflagration and subsonic detonation. The subsonic detonation are only possible for the model with $c_- < c_+$. And the both modes should fulfill that the bubble wall velocity v_w is higher than both v_+ and v_- . The velocity and enthalpy profile of hybrid mode is shown in middle panel of figure. 7.

A.3.1 Supersonic deflagration

Usually, if $c_- < v_w < v_J^{\text{det}}(\alpha_{\bar{\theta}_n})$ the fluid propagate with a supersonic deflagration mode. It should fill the gap between c_- and $v_J^{\text{det}}(\alpha_{\bar{\theta}_n})$. The supersonic deflagration mode can be treated as a superposition of detonation and deflagration, provided the bubble wall is supersonic with respect to the broken phase. The entropy consideration that combines with the hydrodynamic constrains for deflagration and detonation mode enforce $v_- = c_-$. Hence the rarefaction wave behind the bubble wall has to be a Jouguet type. We can derive the following relation to solve eq. (2.16)

$$v_- = c_-, \quad \tilde{v}_- = \mu(v_w, v_-), \quad v_+ = v_J^{\text{def}}(\alpha_{\bar{\theta}_+}), \quad \tilde{v}_+ = \mu(v_w, v_+). \quad (\text{A.12})$$

In our numerical strategy, we first perform the calculation of the deflagration part to give $\alpha_{\bar{\theta}_+}$ and corresponding profiles, then calculate the profile of detonation part as mentioned above.

A.3.2 Subsonic detonation

For the sound velocity of the broken phase c_- is smaller than the sound velocity of the symmetric phase c_+ , we may observe a hydrodynamical mode with $\tilde{v}_- > \tilde{v}_+$ (ie. $v_+ > v_-$). And $v_+ < c_+$, hence in the reference frame of the plasma, the fluid profile propagates with a subsonic mode. Since the constraints of deflagration and detonation and the entropy consideration still apply, we also have the following relation $v_- = c_-$. Therefore the rarefaction wave still propagates with a Jouguet type. From right panel of figure 1, we can observe that only when $\alpha_{\bar{\theta}_+}$ is small enough this hydrodynamical mode can occur. And the stability [32–34] of this mode is still controversial, hence we do not consider this possibility in this study.

References

- [1] P. Amaro-Seoane *et al.* [LISA Collaboration], “Laser Interferometer Space Antenna,” arXiv:1702.00786 [astro-ph.IM].
- [2] C. Caprini *et al.*, “Science with the space-based interferometer eLISA. II: Gravitational waves from cosmological phase transitions,” JCAP **1604**, 001 (2016) [arXiv:1512.06239 [astro-ph.CO]].

- [3] C. Caprini, M. Chala, G. C. Dorsch, M. Hindmarsh, S. J. Huber, T. Konstandin, J. Kozaczuk, G. Nardini, J. M. No and K. Rummukainen, *et al.* “Detecting gravitational waves from cosmological phase transitions with LISA: an update,” *JCAP* **03**, 024 (2020) [arXiv:1910.13125 [astro-ph.CO]].
- [4] <https://www.cosmos.esa.int/web/lisa/lisa-documents>
- [5] J. Luo *et al.* [TianQin Collaboration], “TianQin: a space-borne gravitational wave detector,” *Class. Quant. Grav.* **33**, no. 3, 035010 (2016) [arXiv:1512.02076 [astro-ph.IM]].
- [6] X. C. Hu *et al.*, “Fundamentals of the orbit and response for TianQin,” *Class. Quant. Grav.* **35**, no. 9, 095008 (2018) [arXiv:1803.03368 [gr-qc]].
- [7] J. Mei, Y. Z. Bai, J. Bao, E. Barausse, L. Cai, E. Canuto, B. Cao, W. M. Chen, Y. Chen and Y. W. Ding, *et al.* doi:10.1093/ptep/ptaa114 [arXiv:2008.10332 [gr-qc]].
- [8] W. R. Hu and Y. L. Wu, “The Taiji Program in Space for gravitational wave physics and the nature of gravity,” *Natl. Sci. Rev.* **4**, no. 5, 685 (2017).
- [9] W. H. Ruan, Z. K. Guo, R. G. Cai and Y. Z. Zhang, “Taiji Program: Gravitational-Wave Sources,” arXiv:1807.09495 [gr-qc].
- [10] N. Seto, S. Kawamura and T. Nakamura, “Possibility of direct measurement of the acceleration of the universe using 0.1-Hz band laser interferometer gravitational wave antenna in space,” *Phys. Rev. Lett.* **87**, 221103 (2001) [astro-ph/0108011].
- [11] S. Kawamura *et al.*, “The Japanese space gravitational wave antenna: DECIGO,” *Class. Quant. Grav.* **28**, 094011 (2011).
- [12] H. Kudoh, A. Taruya, T. Hiramatsu and Y. Himemoto, “Detecting a gravitational-wave background with next-generation space interferometers,” *Phys. Rev. D* **73**, 064006 (2006) [gr-qc/0511145].
- [13] V. Corbin and N. J. Cornish, “Detecting the cosmic gravitational wave background with the big bang observer,” *Class. Quant. Grav.* **23**, 2435 (2006) [gr-qc/0512039].
- [14] H. Kurki-Suonio, “Deflagration Bubbles in the Quark - Hadron Phase Transition,” *Nucl. Phys. B* **255**, 231-252 (1985)
- [15] M. Kamionkowski, A. Kosowsky and M. S. Turner, “Gravitational radiation from first order phase transitions,” *Phys. Rev. D* **49**, 2837-2851 (1994) [arXiv:astro-ph/9310044 [astro-ph]].
- [16] H. Kurki-Suonio and M. Laine, “Supersonic deflagrations in cosmological phase transitions,” *Phys. Rev. D* **51**, 5431-5437 (1995) [arXiv:hep-ph/9501216 [hep-ph]].
- [17] J. R. Espinosa, T. Konstandin, J. M. No and G. Servant, “Energy Budget of Cosmological First-order Phase Transitions,” *JCAP* **06**, 028 (2010) [arXiv:1004.4187 [hep-ph]].
- [18] L. Leitaó and A. Megevand, “Spherical and non-spherical bubbles in cosmological phase transitions,” *Nucl. Phys. B* **844**, 450-470 (2011) [arXiv:1010.2134 [astro-ph.CO]].
- [19] L. Leitaó and A. Megevand, “Hydrodynamics of phase transition fronts and the speed of sound in the plasma,” *Nucl. Phys. B* **891**, 159-199 (2015) [arXiv:1410.3875 [hep-ph]].
- [20] M. Hindmarsh and M. Hijazi, “Gravitational waves from first order cosmological phase transitions in the Sound Shell Model,” *JCAP* **12**, 062 (2019) doi:10.1088/1475-7516/2019/12/062 [arXiv:1909.10040 [astro-ph.CO]].
- [21] F. Giese, T. Konstandin and J. van de Vis, “Model-independent energy budget of cosmological first-order phase transitions—A sound argument to go beyond the bag model,” *JCAP* **07**, no.07, 057 (2020) [arXiv:2004.06995 [astro-ph.CO]].
- [22] X. Wang, F. P. Huang and X. Zhang, “Phase transition dynamics and gravitational wave spectra of strong first-order phase transition in supercooled universe,” *JCAP* **05**, 045 (2020) [arXiv:2003.08892 [hep-ph]].

- [23] X. m. Zhang, “Operators analysis for Higgs potential and cosmological bound on Higgs mass,” *Phys. Rev. D* **47**, 3065-3067 (1993) [arXiv:hep-ph/9301277 [hep-ph]].
- [24] C. Grojean, G. Servant and J. D. Wells, “First-order electroweak phase transition in the standard model with a low cutoff,” *Phys. Rev. D* **71**, 036001 (2005) [arXiv:hep-ph/0407019 [hep-ph]].
- [25] F. P. Huang, P. H. Gu, P. F. Yin, Z. H. Yu and X. Zhang, “Testing the electroweak phase transition and electroweak baryogenesis at the LHC and a circular electron-positron collider,” *Phys. Rev. D* **93**, no.10, 103515 (2016) [arXiv:1511.03969 [hep-ph]].
- [26] F. P. Huang, Y. Wan, D. G. Wang, Y. F. Cai and X. Zhang, “Hearing the echoes of electroweak baryogenesis with gravitational wave detectors,” *Phys. Rev. D* **94**, no.4, 041702 (2016) [arXiv:1601.01640 [hep-ph]].
- [27] Q. H. Cao, F. P. Huang, K. P. Xie and X. Zhang, “Testing the electroweak phase transition in scalar extension models at lepton colliders,” *Chin. Phys. C* **42**, no.2, 023103 (2018) [arXiv:1708.04737 [hep-ph]].
- [28] A. Megevand, “Effect of reheating on electroweak baryogenesis,” *Phys. Rev. D* **64**, 027303 (2001) [arXiv:hep-ph/0011019 [hep-ph]].
- [29] X. Wang, F. P. Huang and X. Zhang, “Precise prediction on bubble wall velocity, energy budget and gravitational wave spectrum” work in progress
- [30] A. P. Morais, R. Pasechnik and T. Vieu, “Multi-peaked signatures of primordial gravitational waves from multi-step electroweak phase transition,” [arXiv:1802.10109 [hep-ph]].
- [31] D. Croon and G. White, “Exotic Gravitational Wave Signatures from Simultaneous Phase Transitions,” *JHEP* **05**, 210 (2018) [arXiv:1803.05438 [hep-ph]].
- [32] P. Y. Huet, K. Kajantie, R. G. Leigh, B. H. Liu and L. D. McLerran, “Hydrodynamic stability analysis of burning bubbles in electroweak theory and in QCD,” *Phys. Rev. D* **48**, 2477-2492 (1993) [arXiv:hep-ph/9212224 [hep-ph]].
- [33] A. Megevand and F. A. Membiela, “Stability of cosmological deflagration fronts,” *Phys. Rev. D* **89**, no.10, 103507 (2014) [arXiv:1311.2453 [astro-ph.CO]].
- [34] A. Megevand and F. A. Membiela, “Stability of cosmological detonation fronts,” *Phys. Rev. D* **89**, no.10, 103503 (2014) [arXiv:1402.5791 [astro-ph.CO]].
- [35] F. Giese, T. Konstandin, K. Schmitz and J. van de Vis, “Model-independent energy budget for LISA,” [arXiv:2010.09744 [astro-ph.CO]].